Hydrogen migration in doped and undoped polycrystalline and microcrystalline silicon

N. H. Nickel and I. E. Beckers
Hahn-Meitner-Institut Berlin, Kekuléstr. 5, 12489 Berlin, Germany
(Received 29 March 2002; published 26 August 2002)

Hydrogen diffusion in phosphorous and boron doped polycrystalline and microcrystalline silicon was investigated by deuterium diffusion experiments. Deuterium concentration profiles were measured as a function of temperature, deuterium, and dopant concentrations. The effective diffusion coefficient is thermally activated and varies from 0.01 to 1.69 eV in response to changes in the deuterium and dopant concentrations. This variation is accompanied by a change of the diffusion prefactor by more than 15 orders of magnitude and is even consistent with results reported on H diffusion in hydrogenated amorphous silicon. Using the theoretical diffusion prefactor the energy $\bar{E}_A$ required to yield the diffusion coefficient was calculated. $\bar{E}_A$ reveals a Fermi energy dependence similar to that of the formation energy of H^+ and H^- in *c*-Si. Based upon the experimental data a unified microscopic model for H diffusion is proposed.

DOI: 10.1103/PhysRevB.66.075211 PACS number(s): 61.43.−j, 66.30.−h

I. INTRODUCTION

Although polycrystalline silicon (poly-Si) is used in a wide range of applications ranging from thin-film transistors to solar cells one of its major drawbacks is a high defect concentration after growth[1] that makes it unsuitable for electronic devices. These defects, predominantly located at grain-boundaries, govern the electrical properties of poly-Si. Grain-boundary defects were detected by electron spin resonance and identified as silicon dangling bonds.[2] To obtain technologically useful material these defects must be passivated. Commonly, this is accomplished by exposing poly-Si to a hydrogen plasma at temperatures below 500 °C. The incorporation of hydrogen improves the electrical properties of poly-Si films and devices, for example, by increasing the carrier mobilities and reducing leakage currents.[3,4]

Most of the previous research devoted to hydrogen in poly-Si was focused on the optimization of the H passivation conditions. A variety of hydrogenation sources and techniques such as electron-cyclotron resonance (ECR) plasma, proton implantation, and electrochemical techniques were examined.[5] An enhancement of the hydrogenation efficiency was reported after postultrasound treatments[6] and post-vacuum anneals.[1] Both treatments release H that is not bound to pre-existing Si dangling-bonds.[7] Subsequently, these H atoms can be captured by deep H trapping sites at grain-boundaries lowering the grain-boundary defect concentration.

Hydrogen passivation of poly-Si is governed by the diffusion properties of H atoms.[7] Previous investigations on H diffusion in undoped poly-Si revealed that the diffusion process can be explained in terms of a two-level model[8] that originally was developed to describe diffusion in hydrogenated amorphous silicon.[9,10] Applying the two-level model, information on the H density-of-states was obtained. A distribution of shallow and deep traps was found at 0.5 and 1.5–1.7 eV below the transport level, respectively.[8]

In this paper, the influence of dopants and thus the Fermi energy on hydrogen transport properties in poly-Si and microcrystalline silicon is investigated. Hydrogen diffusion was studied as a function of the phosphorous and boron concentrations, the substrate temperature, and the H concentration. We find that the diffusion activation energy, E_A, depends significantly on the Fermi energy and the H concentration. E_A varies between 0.01 and 1.69 eV, which is accompanied by a change of the diffusion prefactor by more than 15 orders of magnitude.

The paper is organized as follows: Sec. II briefly describes the sample preparation and the hydrogen passivation procedure. Deuterium concentration depth profiles measured by secondary-ion-mass spectrometry (SIMS) are presented in Sec. III. The implications of the data for H diffusion in disordered silicon are discussed in Sec. IV. Finally, Sec. V summarizes the main conclusions of this article.

II. EXPERIMENT

A. Samples

1. Polycrystalline silicon

The experiments described in this paper were performed on phosphorous and boron doped poly-Si films. The samples were prepared by the following procedure. Undoped amorphous silicon was deposited on quartz and on single-crystal silicon wafers covered with a thin thermal oxide by low-pressure chemical vapor deposition (LPCVD) to a thickness of 0.3 μm. Subsequently the samples were crystallized by a furnace anneal in nitrogen atmosphere at 600 °C. Doping was achieved by multiple phosphorous or boron implantations. The dopants were activated in a 30 min furnace anneal at 900 °C. Secondary-ion-mass spectrometry (SIMS) measurements showed that the dopant concentrations are constant with sample thickness. According to transmission electron microscopy (TEM) the resulting poly-Si films are composed of randomly oriented grains with an average grain size of 120 nm.

2. Microcrystalline silicon

Electron-cyclotron resonance chemical vapor deposition (ECRCVD) was used to prepare microcrystalline silicon. Nominally undoped μc-Si and P and B doped specimens were deposited at a substrate temperature of 325 °C using a

 ©2002 The American Physical Society

hydrogen dilution of silane of 98%. Doping was achieved by premixing silane with either B_2H_6 or PH_3. SIMS measurements showed a doping concentration of approximately 10^{20} cm^{-3} for P and the B doped μc-Si. According to Raman measurements all samples used for this study revealed a crystalline fraction of approximately 68%. High-resolution TEM micrographs showed that the specimens were composed of columns with a diameter of approximately 100 nm. These columns are composed of single crystal grains with an average grain-size of ≈15 nm.

B. Hydrogen plasma exposures

Hydrogenation was performed by exposing the samples to monatomic hydrogen generated in an optically isolated remote plasma. The samples were given a metal-oxide-semiconductor grade detergent cleaning, and the native oxide was removed with dilute HF to avoid a barrier to H incorporation. Then the samples were exposed to monatomic H at elevated temperatures. To obtain data at low and high hydrogen concentration diffusion the samples were exposed to monatomic H with and without a stainless steel mesh in the gas stream, respectively. For SIMS analysis deuterium was used as a readily identifiable isotope that duplicates hydrogen chemistry. Since no significant difference in hydrogen and deuterium transport has been found, the terms hydrogenation and deuteration will be used interchangeably in the following discussion.

III. RESULTS

The results presented in this section were obtained by varying the following parameters: the degree of disorder (poly-Si or μc-Si), the dopants (boron and phosphorous) and their concentration, the deuterium concentration, and the substrate temperature. Results obtained on poly-Si and microcrystalline silicon are presented in Secs. III A and III B, respectively. Within each of these sections, the influence of the deuterium and doping concentrations on H diffusion is presented.

A. Polycrystalline silicon

1. High deuterium concentration diffusion

a. Phosphorous doped poly-Si: Typical deuterium concentration profiles in phosphorous doped poly-Si are shown in Fig. 1. The samples were exposed to monatomic deuterium for 5 min at the indicated temperatures. With increasing substrate temperature, T_H, deuterium diffuses deeper into the bulk. At low temperatures the deuterium concentration decreases exponentially with depth with a characteristic slope of $x_0 \approx 24$ nm. At $T_H \geqslant 206\,°$C the deuterium concentration decreases according to a complementary error function, erfc. Within the first 50 nm the deuterium depth profiles exhibit a surface peak indicated by the dotted curve in Fig. 1. In phosphorous doped poly-Si the D accumulation in the near-surface region is attributed to the presence of deuterium stabilized platelets.[11,12] The increasing temperature also results in an increase of the D surface concentration, C_0. This is in contrast to previous diffusion studies on undoped poly-Si, where an increase of the passivation temperature was accompanied by a decrease of C_0.[8] However, this is not related to the presence of dopants but to the difference in the hydrogenation time. In Fig. 2 the deuterium surface concentration is plotted as a function of the deuteration time, t. With increasing deuteration time C_0 increases until the H chemical potential in the plasma equilibrates with the H chemical potential in the poly-Si film. At a temperature of 200 °C this occurs after an exposure for 900 s. At lower temperatures the time to reach the equilibrium increases since the equilibration process is governed by diffusion. Hence, a decrease of C_0 with increasing temperature is expected for longer passivation times ($t > 2000$ s) similar to that observed for D diffusion in undoped poly-Si.[8]

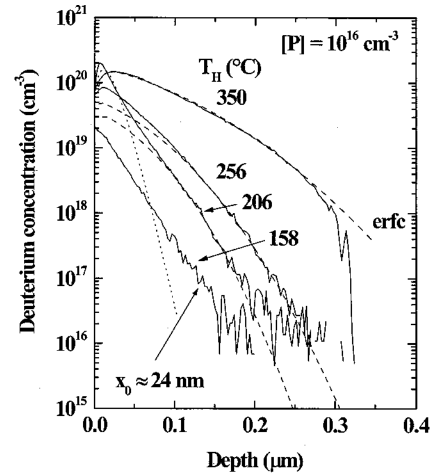

FIG. 1. Deuterium concentration depth profiles in polycrystalline silicon (solid lines) doped with a phosphorous concentration of 10^{16} cm^{-3}. The specimens were exposed to monatomic D for 5 min at the indicated temperatures. The dashed lines depict a least-squares fit to the convolution of an erfc with the SIMS depth resolution function (Ref. 9). The dotted curve sketches the accumulation of deuterium close to the sample surface.

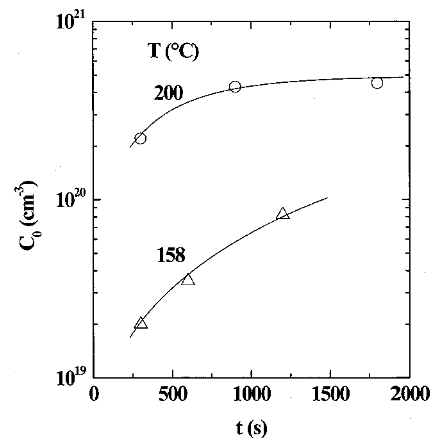

FIG. 2. Deuterium surface concentration, C_0, as a function of the deuteration time for the indicated substrate temperatures. The poly-Si films were doped with a phosphorous concentration of 10^{16} cm^{-3}.

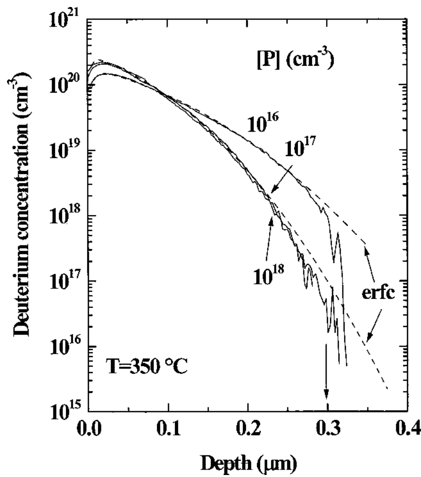

FIG. 3. Deuterium concentration depth profiles in poly-Si doped with the indicated phosphorous concentrations. The specimens were exposed to monatomic D for 5 min at 350 °C. The dashed lines depict a least-squares fit to the convolution of an erfc with the SIMS depth resolution function (Ref. 9). The arrow indicates the interface between the poly-Si layer and the substrate.

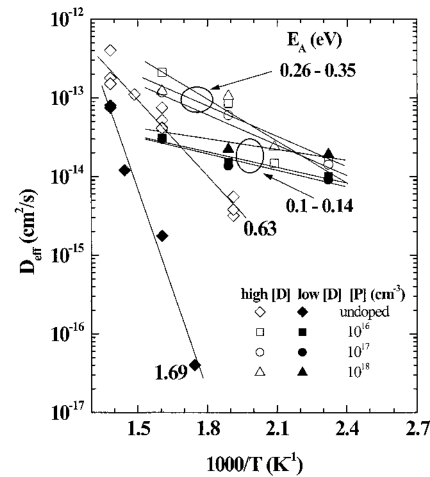

FIG. 4. Effective diffusion-coefficient, D_{eff}, as a function of the reciprocal temperature for high (open symbols) and low (solid symbols) D concentration diffusion. The squares, circles, and triangles represent diffusion coefficients in phosphorous doped poly-Si with P concentrations of 10^{16}, 10^{17}, and 10^{18} cm^{-3}, respectively. The diamonds represent D_{eff} in undoped poly-Si from Ref. 8.

The influence of the phosphorous concentration on the D concentration depth profiles is shown in Fig. 3. Simultaneously, the samples were exposed to monatomic D at 350 °C for 5 min. The poly-Si film doped with a phosphorous concentration of 10^{16} cm^{-3} reveals the highest D concentration at the poly-Si/substrate interface (arrow in Fig. 3). With increasing P concentration deuterium diffusion decreases and specimens doped with a P concentration of 10^{17} and 10^{18} cm^{-3} reveal identical D depth profiles. A similar but more pronounced influence of the doping concentration on deuterium diffusion in single crystal silicon (*c*-Si) was reported previously.[13] As an explanation Herring and Johnson[13] suggested that as the doping concentration increases, the surface concentration of the dominating diffusion species decreases since more and more hydrogen interacts with dopants and forms complexes.

The effective diffusion coefficient, D_{eff}, and the deuterium surface concentration were obtained from least-squares fits of the data to the convolution of a complementary error function and the resolution function of the SIMS analysis.[9] In Fig. 4 the effective diffusion-coefficient is plotted as a function of the reciprocal temperature (open symbols). D_{eff} shows an apparent activation energy varying between $E_A = 0.26$ and 0.35 eV. An increase of the phosphorous concentration from 10^{16} to 10^{18} cm^{-3} does not result in a significant change of E_A. Compared to deuterium diffusion in undoped poly-Si (open diamonds),[8] the presence of phosphorous results in a decrease of E_A by about 0.3 eV. Moreover, P doping of poly-Si results in an enhancement of D_{eff}, e.g., in P doped poly-Si the effective diffusion-coefficient exceeds D_{eff} of undoped material by approximately a factor of 25 at 250 °C.

b. Boron doped poly-Si: Deuterium concentration depth profiles in boron doped poly-Si are shown in Fig. 5. The specimens were deuterated at the indicated temperatures for 5 min. At low hydrogenation temperatures ($T \leq 206$ °C) the D depth profiles decay exponentially with depth with a characteristic decay length of approximately 27 nm. At higher temperatures the depth profiles decay according to an erfc. This behavior is similar to D diffusion in phosphorous doped poly-Si. However, deuterium diffusion in B doped poly-Si is enhanced compared to diffusion in P doped samples (compare Figs. 1 and 5). In Fig. 6 the temperature dependence of the D concentration depth profiles is shown for poly-Si films doped with a boron concentration of 10^{18} cm^{-3}. The data show that an increase in the boron concentration results in an enhancement of the deuterium diffusion. It is interesting to

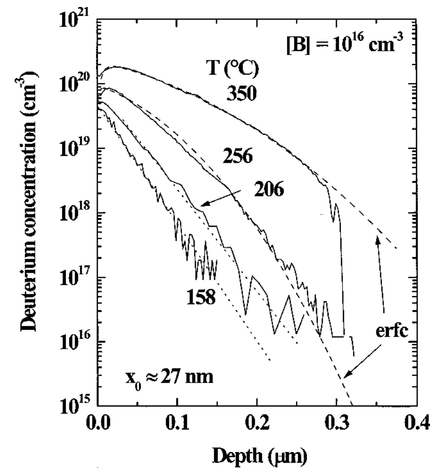

FIG. 5. Deuterium concentration depth profiles in boron doped poly-Si (solid lines). The boron concentration amounts to 10^{16} cm^{-3}. The specimens were exposed to monatomic D for 5 min at the indicated temperatures. The dashed lines depict a least-squares fit to the convolution of an erfc with the SIMS depth resolution function (Ref. 9). The dotted lines indicate the exponential decays with a characteristic length of $x_0 \approx 27$ nm.

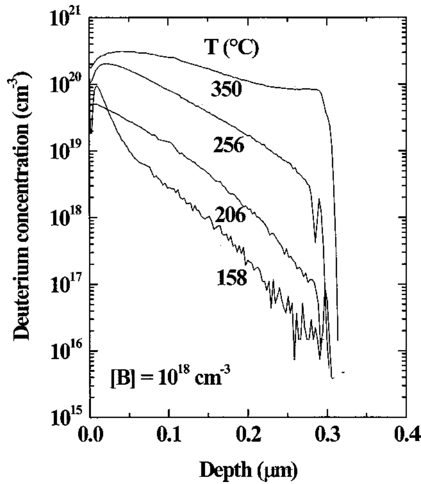

FIG. 6. Deuterium concentration depth profiles in poly-Si doped with a boron concentration of 10^{18} cm^{-3}. The samples were exposed to monatomic D for 5 min at the indicated temperatures.

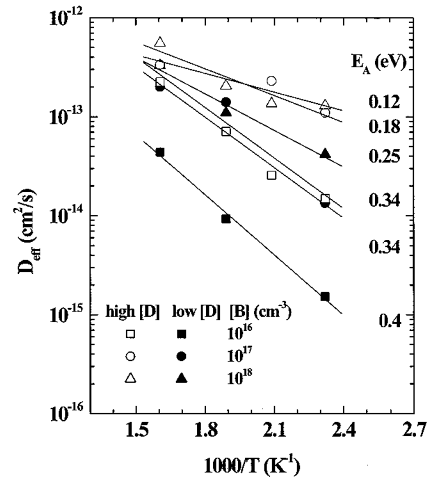

FIG. 7. Effective diffusion-coefficient, $D_{\rm eff}$, as a function of the reciprocal temperature for high (open symbols) and low (solid symbols) D concentration diffusion. The squares, circles, and triangles represent diffusion coefficients in boron doped poly-Si with B concentrations of 10^{16}, 10^{17}, and 10^{18} cm^{-3}, respectively.

note that the specimen deuterated at 158 °C reveals a D accumulation in the near-surface region similar to that of phosphorous doped specimens. In this case, however, the D accumulation is not due to the presence of platelets since platelets are only observed in undoped and n-type material.[11,12] In case of boron doped poly-Si the D accumulation in the near-surface region could be due to the formation of other deuterium complexes such as interstitial molecular D_2 or B–D.

The temperature dependence of $D_{\rm eff}$ for various boron concentrations is shown by the open symbols in Fig. 7. The apparent activation energy of $D_{\rm eff}$ decreases from $E_A=0.34$ to 0.12 eV as the B concentration increases from 10^{16} to 10^{18} cm^{-3}. The decrease of the activation energy with increasing doping concentration is more pronounced in boron doped poly-Si than in phosphorous doped material. Also, comparing the effective diffusion coefficients for P and B doped poly-Si reveals that $D_{\rm eff}$ in p-type samples exceeds $D_{\rm eff}$ in n-type samples by about a factor of 3–6 (open circles and triangles in Figs. 4 and 7). These results indicate that the presence of either free electrons or holes plays an important role in the microscopic diffusion process of hydrogen.

2. Diffusion from an attenuated plasma

In the diffusion experiments discussed in the previous section, a change in the deuterium concentration occurred always in conjunction with a change in the deuteration temperature. In order to study the influence of the deuterium concentration on the diffusion properties separately, the D surface concentration, and thus the D flux into the specimens, was attenuated by inserting a stainless steel mesh into the monatomic deuterium flux. In Fig. 8 the curves labeled "attenuated" represent typical D concentration depth profiles in phosphorous doped poly-Si obtained after a 5 min exposure to an attenuated deuterium plasma at 350 °C. The curves labeled "normal" represent D depth profiles in P-doped and undoped samples without attenuating the deuterium flux. Attenuation of the D flux results in a decrease of the D surface concentration by about two orders of magnitude which is independent of the phosphorous concentration. Furthermore, the deuterium concentration profiles decay exponentially with depth with a characteristic slope of $x_0=34$ nm. The decrease of the D concentration is accompanied by a decrease of the effective diffusion coefficient by a factor of 5–7. Similar results were obtained at lower deuteration temperatures. The temperature dependence of $D_{\rm eff}$ is shown by the solid symbols in Fig. 4. The effective diffusion coefficient is thermally activated with an activation energy of $E_A=0.1-0.14$ eV. Compared with low D concentration diffusion in undoped poly-Si (solid diamonds in Fig. 4) phosphorous doping results in a decrease of E_A by approximately 1.6 eV.

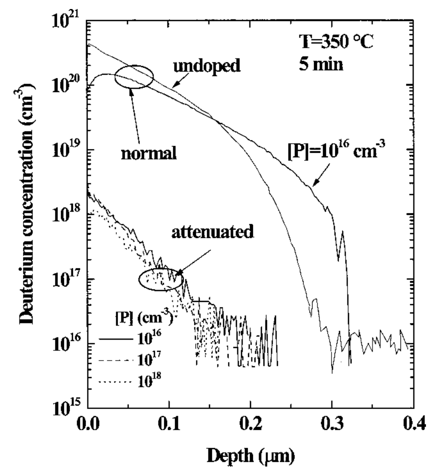

FIG. 8. Deuterium concentration depth profiles in undoped and P doped poly-Si after a plasma exposure for 5 min at 350 °C. The curves labeled "normal" display the D concentration profile after a standard plasma exposure, and the profiles labeled "attenuated" were obtained by attenuating the D flux into the specimens using a stainless steel mesh.

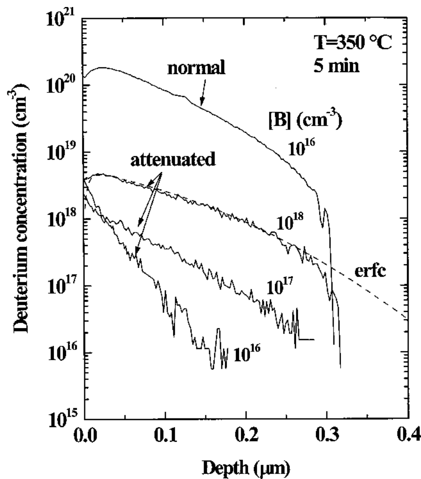

FIG. 9. Deuterium concentration depth profiles in boron doped poly-Si after a plasma exposure for 5 min at 350 °C. The curve labeled ''normal'' displays the D concentration profile after a standard plasma exposure, and the profiles labeled ''attenuated'' were obtained by attenuating the D flux into the specimens using a stainless steel mesh.

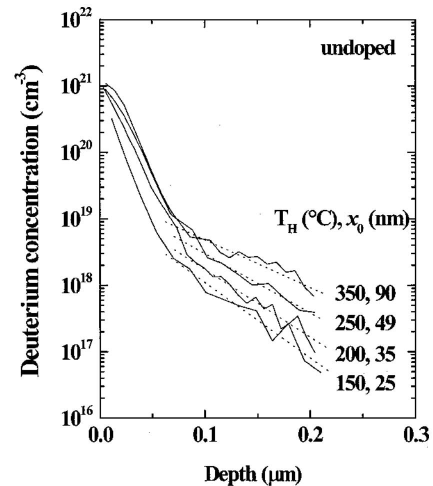

FIG. 10. Deuterium concentration depth profiles in undoped μc-Si. The specimens were exposed to monatomic D for 4 min at the indicated temperatures.

Identical low concentration diffusion experiments were carried out in boron doped poly-Si samples. D depth profiles, measured after an exposure to an attenuated D plasma at 350 °C for 5 min, are plotted in Fig. 9. Similar to P doped samples the D surface concentration decreases by about 2 orders of magnitude. However, only for the lowest boron concentration the depth profiles exhibit an exponential decay with $x_0 \approx 18$ nm. With increasing B concentration the deuterium concentration in the bulk of the specimens increases and the depth profiles decay according to an erfc with depth. This is accompanied by an increase of D_{eff} with increasing B concentration. The concentration dependence of D_{eff} is less pronounced in boron doped material than in phosphorous doped and undoped[8] poly-Si. From the data presented above it can be concluded that the concentration dependence of D_{eff} is important for understanding the microscopic processes that govern H diffusion in disordered silicon.

B. Microcrystalline silicon

1. High deuterium concentration diffusion

a. Undoped microcrystalline silicon: The influence of the host material on hydrogen diffusion properties was investigated by repeating the diffusion experiments in microcrystalline silicon (μc-Si). The main differences to poly-Si are the crystalline structure and an average hydrogen content of 6.5 at. % in the as-grown material.[14]

Deuterium concentration profiles measured in nominally undoped μc-Si are plotted in Fig. 10. In contrast to D depth profiles measured in poly-Si (see above) the data in Fig. 10 exhibit a kink at a depth of approximately 70 nm. A similar behavior was reported for H diffusion in LPCVD-grown poly-Si, previously.[8] For D concentrations above 10^{19} cm^{-3} the temperature dependence of D diffusion is infinitely small. This is in contrast to the temperature dependence of low D-concentration diffusion. The D concentration decays exponentially with depth and with increasing passivation temperature the characteristic slope x_0 increases from ≈ 25 to ≈ 90 nm.

The accumulation of D in the near-surface region is similar to that observed for n-type poly-Si (Fig. 1) suggesting the presence of H stabilized platelets. This is consistent with n-type conductivity and a Fermi energy in the upper half of the band gap typically observed in nominally undoped μc-Si. The fast diffusion component at low D concentrations most likely is due to the structural composition of the samples. While grain boundaries act as efficient sinks for H and diminish the diffusivity,[8,15] microcrystalline silicon, and LPCVD-grown poly-Si consist of columnar grains that act as diffusion pipes due to a lack of grain boundaries perpendicular to the columns.[8]

The temperature dependence of the effective diffusion coefficient is shown by the open triangles in Fig. 11. High concentration H diffusion reveals an activated behavior with $E_A \approx 0.29$ eV for nominally undoped μc-Si. Because the samples show n-type conductivity, with a Fermi energy of $E_c - E_F \approx 0.3$ eV, the activation energy has to be compared with E_A of P-doped poly-Si. In poly-Si (Fig. 4) E_A decreases from 0.35 to 0.26 eV with increasing P concentration. These values are similar to E_A for high H concentration diffusion in nominally undoped microcrystalline silicon.

b. Phosphorous doped microcrystalline silicon: Deuterium concentration depth profiles in phosphorous doped μc-Si are shown in Fig. 12. At low temperatures ($\leqslant 200$ °C) the depth profiles are independent of the passivation temperature. At higher temperatures D diffuses somewhat deeper into the sample. Compared with D diffusion in phosphorous doped poly-Si, diffusion in μc-Si is strongly diminished (see Figs. 1 and 3). Moreover, for all passivation temperatures, the concentration depth profiles in Fig. 12 decay exponentially with depth with a characteristic slope of $x_0 \approx 8$ nm. However, this low value of x_0 is determined by the SIMS

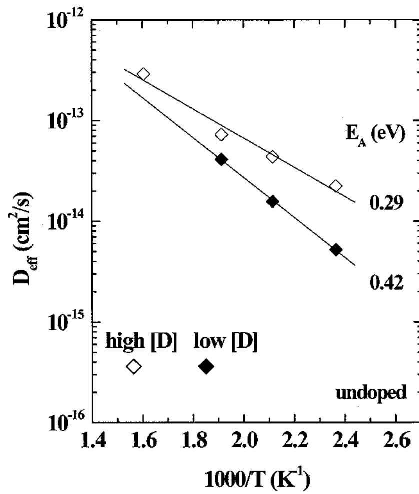

FIG. 11. Temperature dependence of $D_{\rm eff}$ in nominally undoped μc-Si for high (open symbols) and low (solid symbols) D concentration diffusion.

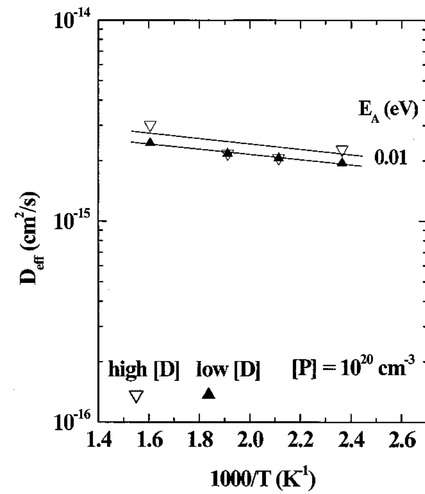

FIG. 13. Effective diffusion-coefficient, $D_{\rm eff}$, as a function of the reciprocal temperature for high (open triangles) and low (solid triangles) D concentration diffusion. The samples were doped with a phosphorous concentration of 10^{20} cm^{-3}.

depth resolution.

Figure 13 shows the temperature dependence of the effective diffusion coefficient. The open triangles represent $D_{\rm eff}$ for high D concentration diffusion. The activation energy of $E_A \approx 0.01$ eV obtained from a least squares fit of the data indicates that H diffusion in highly phosphorous doped μc-Si is independent of temperature up to 350 °C. This indicates that all D atoms entering the specimens are trapped in the near-surface region forming complexes most likely with phosphorous atoms.[13] Since the P concentration in μc-Si exceeds the P concentration in poly-Si by 2 orders of magnitude it is conceivable that H diffusion in poly-Si doped with the same P concentration would show a similar temperature dependence of $D_{\rm eff}$.

c. Boron doped microcrystalline silicon: Deuterium concentration profiles measured in boron doped microcrystalline silicon are shown in Fig. 14. For all passivation temperatures a D accumulation in the near-surface region (depth $\leqslant 0.1$ μm) is observed. As in poly-Si, the D accumulation is not related to the presence of platelets, but most likely, the D accumulation is due to the formation of D complexes such as interstitial H_2 or BH. Compared with undoped and phosphorous doped μc-Si, diffusion in boron doped samples is enhanced. At temperatures above 200 °C and a D concentration of approximately 2×10^{18} cm^{-3} the deuterium profiles exhibit a kink and deviate from the erfc fits. The D concentration decays exponentially with a characteristic slope of $\approx$73–90 nm.

In Fig. 15 the open triangles represent $D_{\rm eff}$ for high D concentration diffusion. The small activation energy of $E_A \approx 0.07$ eV indicates that H diffusion in highly boron doped μc-Si is independent of temperature in the accessible temperature range.

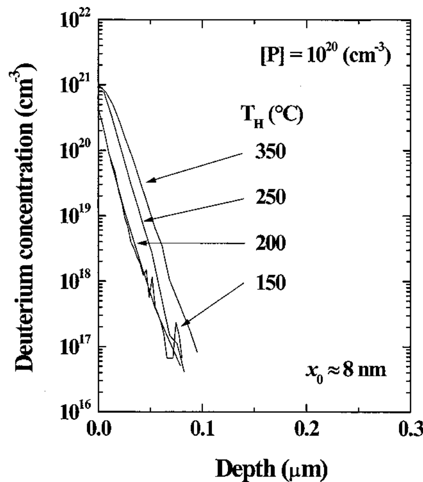

FIG. 12. D concentration depth profiles in P doped μc-Si. The samples were deuterated for 4 min at the indicated temperatures.

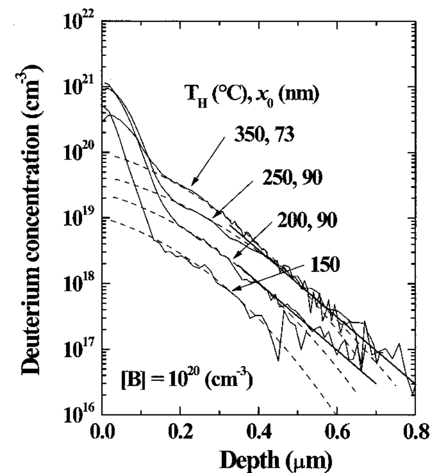

FIG. 14. Deuterium concentration depth profiles in boron doped μc-Si. The dashed lines depict a least-squares fit to an erfc and the thick solid lines indicate an exponential decay of the D concentration. The specimens were exposed to monatomic D for 4 min at the indicated temperatures.

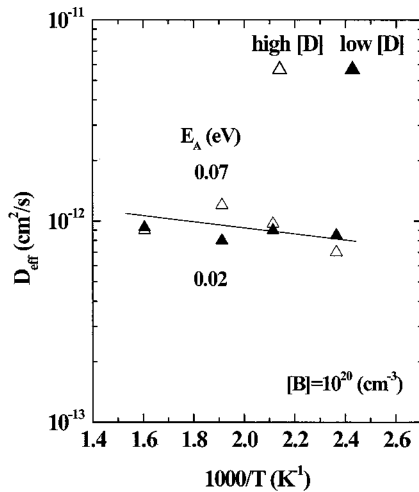

FIG. 15. D_{eff} as a function of the reciprocal temperature for high (open triangles) and low (solid triangles) D concentration diffusion. The samples were doped with a boron concentration of 10^{20} cm^{-3}.

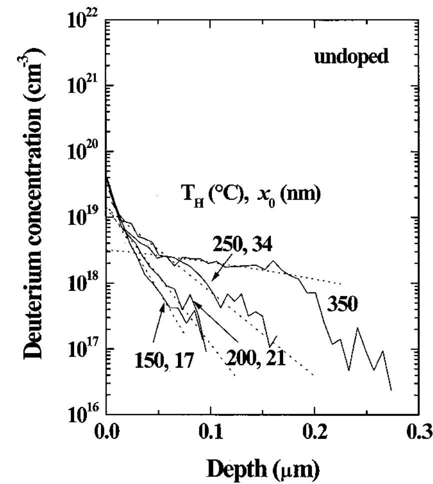

FIG. 16. Deuterium concentration depth profiles in undoped μc-Si after a 4 min plasma exposure at the indicated substrate temperatures. The D plasma was attenuated using a stainless steal mesh.

2. Diffusion from an attenuated plasma

In this subsection we present data obtained from low H concentration diffusion experiments in doped and undoped microcrystalline silicon. Undoped, P-, and B-doped μc-Si samples were exposed to an attenuated D plasma, simultaneously. The temperature dependence of the D depth distribution in undoped μc-Si is shown in Fig. 16. Compared with data from a normal plasma exposure (Fig. 10) the deuterium surface concentration decreased by almost 2 orders of magnitude. In addition, plasma attenuation prevents the accumulation of large amounts of D in the subsurface region ($depth < 0.1$ μm). The D concentration decreases exponentially with depth and x_0 increases with increasing temperature. However, the values of x_0 are somewhat smaller compared with those obtained from normal plasma exposure (Fig. 10).

The temperature dependence of D_{eff} is depicted by the solid squares in Fig. 11. The data indicate activated behavior with $E_A \approx 0.42$ eV. This activation energy is larger than E_A in n-type poly-Si (see Fig. 4).

Low concentration deuterium depth profiles in phosphorous doped μc-Si are shown in Fig. 17. Again, plasma attenuation resulted in a pronounced decrease of the D surface concentration. For all temperatures the D concentration decreases exponentially with depth and $x_0 \approx 8$ nm reflects the SIMS depth resolution. The temperature dependence of the effective diffusion coefficient is depicted by the solid triangles in Fig. 13. In the experimentally accessible temperature range D_{eff} is independent of temperature. The effective diffusion coefficients for high and low concentration diffusion are alike suggesting that the governing diffusion mechanism is complex formation with dopants.[13]

Figure 18 shows D depth profiles in B doped μc-Si after an exposure to an attenuated D plasma for 4 min at the indicated temperatures. As in the other specimens, plasma attenuation resulted in a decrease of the D surface concentration. In addition, the near surface peak, observed for high D concentration diffusion, disappeared. However, despite an attenuated D plasma the depth distributions for low and high D concentration diffusion are comparable. This becomes also evident when comparing the effective diffusion coefficients. The values of D_{eff} for high (open symbols) and low (solid symbols) D concentration diffusion amount to approximately 10^{-12} cm^2/s independent of temperature (Fig. 15).

Similar to H migration in poly-Si the results presented in this section demonstrate that H diffusion in μc-Si is very sensitive to doping and thus, to the position of the Fermi energy. Diffusion in boron doped μc-Si is enhanced compared with nominally undoped and phosphorous doped material. Moreover, in highly doped μc-Si the effective diffusion coefficient is independent of temperature for high and low D concentration diffusion. Most likely this is due to an enhanced H complex formation rate with phosphorous or boron.

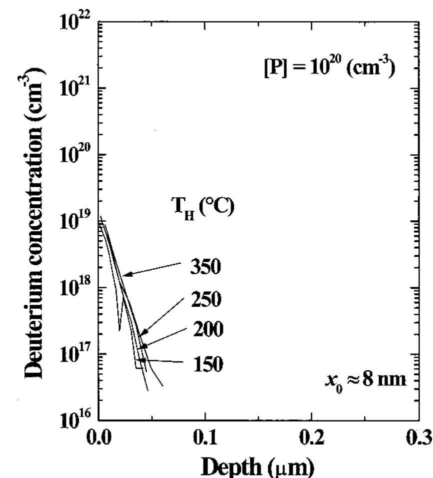

FIG. 17. Deuterium concentration depth profiles in phosphorous doped μc-Si after a 4 min plasma exposure at the indicated substrate temperatures. The D plasma was attenuated using a stainless steal mesh.

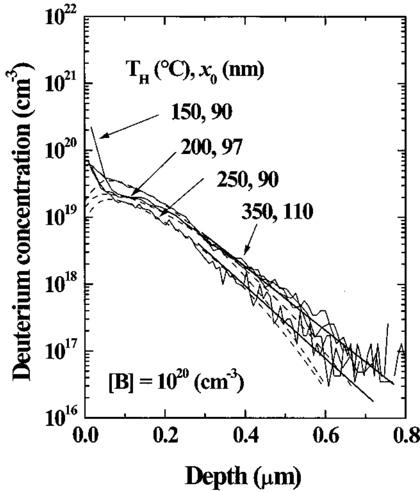

FIG. 18. Deuterium concentration depth profiles in boron doped μc-Si after an exposure to an attenuated plasma for 4 min at the indicated temperatures. The dashed lines depict least-squares fits to the convolution of an erfc and the SIMS depth resolution. The thick solid lines indicate an exponential decay of the D concentration.

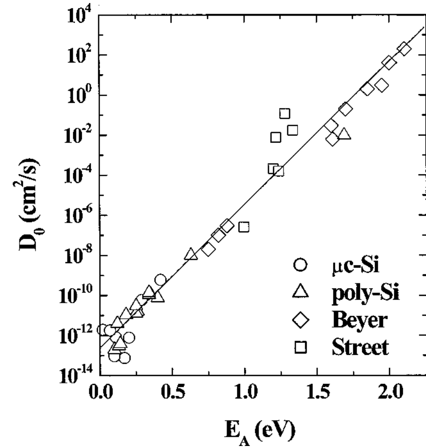

FIG. 19. Diffusion prefactor D_0 vs activation energy E_A. The triangles and circles represent poly-Si and μc-Si data from this work. The diamonds and squares are obtained from diffusion data in amorphous silicon (Refs. 17, 18).

IV. DISCUSSION

A. Temperature dependence of the diffusion coefficient

In the past, two significantly different models were proposed for hydrogen diffusion in amorphous and polycrystalline silicon. The *equilibrium model* assumes that hydrogen motion is a quasiequilibrium process where the hydrogen chemical potential defines the filling level of the H density-of-states and determines the concentration of hydrogen atoms in the transport states. This model does not require the presence of deep hydrogen traps.[16,17] On the other hand, the *trapping model* is based on the assumption that shallow and deep hydrogen states are not in equilibrium. Hydrogen in the shallow or transport states is trapped and released as it migrates through the semiconductor. Hydrogen equilibrates within the shallow trap distribution during typical diffusion-experiment time scales. Separated in energy from these states are deep hydrogen states. These traps capture and release hydrogen on time scales long compared to the diffusion experiments. The hydrogen chemical potential separates the filled from the empty states.[8–10] Model parameters such as the energy of deep trapping sites with respect to the transport states are estimated from the temperature dependence of the hydrogen diffusion. In analogy to charge transport it is assumed that in a simple hydrogen density-of-states distribution the effective diffusion coefficient is given by

$$D_{\mathrm{eff}}=D_0 \exp\left(-\frac{E_A}{kT}\right), \tag{1}$$

with a prefactor D_0, an activation energy E_A, the temperature T, and the Boltzmann constant k. Previously, it was argued that this equation is valid even for broadened density-of-states which exhibit peaks in the occupied densities-of-states centered at various band energies, and therefore E_A should correspond to the energies of shallow and deep trapping levels.[8,9] In this approach the key assumption is a prefactor D_0 that is independent of experimental parameters such as hydrogen concentration, H density-of-states distribution, Fermi energy, and macroscopic structure (amorphous, micro-, or polycrystalline).

The prefactor D_0 was estimated by extrapolating the temperature dependence of D_{eff} (Figs. 4, 7, 11, 13, and 15) to $1/T=0\ \mathrm{K}^{-1}$. In Fig. 19, D_0 is plotted as a function of the activation energy E_A. The circles and triangles depict data from μc-Si and poly-Si, respectively. In addition, D_0 and E_A data from hydrogen diffusion experiments performed in *a*-Si:H are included from Refs. 18 and 19. With increasing activation energy D_0 increases by more than 15 orders of magnitude. Moreover, it is striking that all data points lie on a straight line independent of the degree of disorder in the host material (*a*-Si:H, μc-Si, poly-Si). This phenomenon is well known as Meyer–Neldel behavior[20] and has been observed for hydrogen diffusion in *a*-Si:H, previously.[21] The data plotted in Fig. 19 clearly show that the prefactor D_0 depends on the experimental conditions. Hence, the activation energies obtained from the temperature dependence of D_{eff} do not correspond to the energy of deep or shallow H trapping sites.

To elucidate the microscopic mechanism of hydrogen diffusion, we propose the following analysis of the diffusion data. Theoretically, the diffusion prefactor, D_0, should be independent of H concentration, dopant concentration, and the degree of disorder of the host material. The microscopic diffusion prefactor is given by $D_0^t=1/6\nu a^2$, where ν is the attempt frequency and a is the mean free path. Reasonable assumptions of $\nu\approx 10^{12}$ Hz and $a\approx 0.3$ nm lead to an estimate of the theoretical diffusion prefactor of $D_0^t \approx 10^{-3}\ \mathrm{cm}^2/\mathrm{s}$. With this prefactor the diffusion activation energy can be calculated using the relation,

$$\bar{E}_A=-kT \ln\left(\frac{D_{\mathrm{eff}}}{D_0^t}\right). \tag{2}$$

In Fig. 20, $\bar{E}_A$ at $T=350\,^{\circ}\mathrm{C}$ is plotted as a function of the Fermi energy. The solid triangles represent poly-Si data

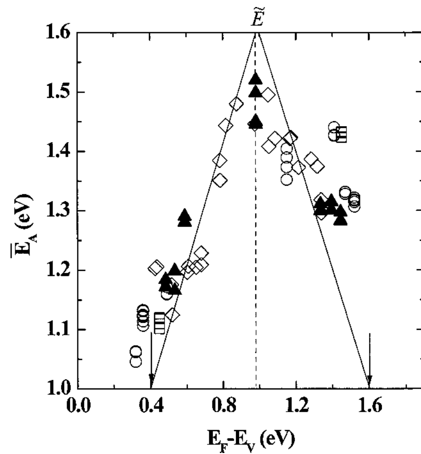

FIG. 20. $\bar{E}_A$ as a function of the Fermi energy at 350 °C. Data obtained from μc-Si are shown by squares. The circles and diamonds were obtained for H diffusion in *a*-Si:H from Refs. 18 and 19, respectively, after analyzing the data according to Eq. (2). $\tilde{E}$ denotes the mean energy of the electronic states of H^+ and H^- in silicon. The arrows indicate the approximate positions of conduction and valence bands of poly-Si and μc-Si with respect to the band gap of *a*-Si:H.

while the squares depict data from H diffusion in microcrystalline silicon. In addition, temperature dependent diffusion data on doped and undoped *a*-Si:H from Refs. 18 (circles) and 19 (diamonds) were analyzed according to Eq. (2) and included in the plot. The band offsets for *a*-Si:H, poly-Si, and μc-Si were estimated using the following procedure. For *a*-Si:H and poly-Si $\bar{E}_A$ increases as the Fermi energy moves away from the band edges. The maximum of $\bar{E}_A$ occurs at $E_F - E_V \approx 0.98$ and ≈ 0.58 eV in *a*-Si:H and poly-Si, respectively. In poly-Si this value coincides with the mean energy, $\tilde{E}$, for the electronic states of H^+ and H^- complexes in single crystal silicon.[22] The band gaps of *a*-Si:H and poly-Si were adjusted at $\tilde{E}$. This leads to a reasonable conduction-band offset of approximately 0.4 eV for amorphous and polycrystalline silicon. Arrows in Fig. 20 indicate the positions of the conduction and valence bands of poly-Si.

Independent of the host material $\bar{E}_A$ exhibits a significant dependence on the Fermi energy. $\bar{E}_A$ increases from ≈ 1.05 to 1.5 eV and then decreases to ≈ 1.3 eV as the Fermi energy moves from the valence band to the conduction band. It is interesting to note that the observed change of $\bar{E}_A$ with the Fermi energy is comparable to that of the formation energy, E_{form}, for H^+ and H^-; the latter quantity changes with a slope of $+1$ and -1 for H^+ and H^-, respectively.[23]

Previously, it was assumed that $\bar{E}_A$ represents an estimate of the hydrogen chemical potential with respect to the H transport states, namely $E_{\mathrm{M}} - \mu_{\mathrm{H}}$.[8,17] The H chemical potential is determined by the occupation of the H density-of-states distribution and the quasichemical potential of the monatomic H gas assuming that H in the solid is in approximate equilibrium with the monatomic H in the plasma gas. This allows the estimate of trap levels and the position of the H chemical potential within the context of a two-band model using the temperature and time dependence of H diffusion. In the following discussion we propose a different interpretation of $\bar{E}_A$ taking into account the charge state of the migrating H species, trapping and release of H from deep trapping sites, and the influence of the hydrogen chemical potential.

B. Diffusion of charged hydrogen

The charge state of hydrogen plays an important role for the microscopic diffusion process. From hydrogen diffusion and drift studies in *c*-Si and first-principles calculations it is known that monatomic H diffuses in the positive (H^+) and negative charge state (H^-) in *p*-type and *n*-type silicon, respectively.[23–25] The lowest-energy state of H in silicon is formed by exchanging electrons with the Fermi level. Thus, the formation energies of charged hydrogen depend on the Fermi energy. For instance, to change the charge state of a neutral hydrogen (H^0) to a negatively charged atom (H^-) an electron has to be removed from the Fermi level to the H^0. In *p*-type silicon this process costs more energy than in *n*-type samples. Therefore, the negative charge state will be more stable in *n*-type silicon. The neutral charge state is never stable which is characteristic for a ‘‘negative-*U*’’ center. The dashed line labeled $\tilde{E}$ in Fig. 20 indicates the Fermi energy at which monatomic H changes from being nearly all positive (H^+) to nearly all negative (H^-); in *c*-Si and poly-Si $\tilde{E}$ resides at $E_c - 0.4$ eV.[22]

Hydrogen transport occurs by surmounting a barrier between minimum energy positions. According to first-principles calculations, in *n*-type *c*-Si the global minimum is the tetrahedral interstitial site, T_d, with a migration barrier of $E_m = 0.25$ eV between T_d sites. On the other hand, in *p*-type silicon the bond-centered site (BC), was identified as the global minimum with $E_m = 0.2$ eV.[23] These migration barriers are slightly smaller than the activation energy of 0.5 eV obtained from high temperature diffusion experiments of H^+.[26] Once hydrogen diffuses in the transport states the diffusion activation energy in disordered silicon (poly-Si, μc-Si, *a*-Si:H) should be the same as in *c*-Si since the short range order in disordered silicon is similar to that in *c*-Si. In fact, *in situ* conductivity measurements performed during plasma hydrogenation showed that in intrinsic and *p*-type poly-Si hydrogen diffuses in the positive charge state.[27] Moreover, since the charge state does not change along the diffusion path,[23] the diffusion barrier remains independent of the Fermi energy for H^+ as well as for H^-. Hence, the observed Fermi energy dependence of $\bar{E}_A$ should be attributed to a Fermi level dependence of the formation energy of interstitial hydrogen.

The experimentally observed activation energies for H diffusion in disordered silicon are significantly higher than the migration barriers for interstitial H. This is indicative of H capture and release at deep states. In *c*-Si hydrogen is known to form large two-dimensional clusters,[11,28] interstitial diatomic H_2,[29] and H-dopant complexes[13] that slow down the diffusion process. Disordered silicon provides additional prominent deep H traps namely, silicon dangling bonds.[2,7] The presence of deep H traps results in a significant decrease

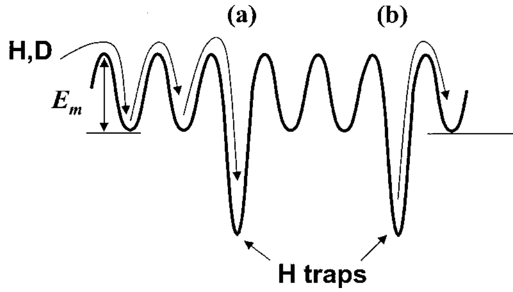

FIG. 21. Illustration of the microscopic diffusion mechanism of H and D atoms in disordered silicon. E_m is the migration barrier for interstitial diffusion. (a) and (b) illustrate H trapping and detrapping at a deep site, respectively.

of the diffusivity; grain boundaries in poly-Si act as efficient traps for H and D, effectively reducing the diffusivity.[8,15] Thus, the microscopic diffusion process can be described by three processes: (i) migration of charged interstitial H in the transport states over a barrier E_m, (ii) capture of H at deep trapping sites, and (iii) the release of H from deep states into interstitial transport states. These processes are sketched in Fig. 21. In the following example we will consider H^+ diffusion in *p*-type samples; the microscopic picture for H^- diffusion is equivalent. In undoped and *p*-type samples H diffuses in the positive charge-state H^+. When H^+ is captured in a deep trapping site, like a Si dangling bond, the capture of an electron is required to form a Si–H bond. Dissociation of this complex occurs through the wagging vibration of the Si–H bond. When the H atom approaches the adjacent Si–Si bond center defect levels move from the conduction and valence bands into the gap. These states can capture charge upon which the Si–H bond dissociates[30] leaving behind a Si dangling-bond and a neutral H. The *p*-type nature of the semiconductor requires a change of the charge state to H^+. The latter mechanism should account for the dependence of $\bar{E}_A$ on the Fermi energy. However, if the Fermi energy is close to the valence band a second charge transfer from the Si dangling bond should occur to form a positively charged defect. Accordingly, $\bar{E}_A$ should change twice as fast in response to a shift of the Fermi energy; the slopes of the lines in Fig. 20 should be +2 and −2. This, however, is not the case. Possible reasons might be potential fluctuations at grain boundaries or temperature dependence of the theoretical diffusion prefactor, D_0^t.

An important result comes from electron paramagnetic resonance (EPR) measurements performed on phosphorous, boron, and undoped poly-Si. The P and B concentrations of the investigated samples were about 10^{18} cm^{-3}. Independent of the doping concentration the Si dangling bond concentration varied between 5×10^{18} and 7.7×10^{18} cm^{-3}. This observation demonstrates that a change of the Fermi energy does not result in a change of the charge state of Si dangling bonds.[31] Therefore, the following microscopic picture evolves for poly-Si and μc-Si:H. A Si–H bond dissociates into a neutral Si dangling bond and a neutral H atom. Subsequently, only the charge state of the H atom changes into H^+ or H^- depending on the Fermi energy of the semiconductor. The latter process is reflected by the Fermi energy dependence of $\bar{E}_A$ with slopes of +1 and −1 for $E_F-E_V<\tilde{E}$ and $E_F-E_V\geqslant\tilde{E}$, respectively, as observed in Fig. 20.

$\bar{E}_A$ can be written as

$$\bar{E}_A=E_m+E_{\mathrm{form}}(\mathrm{H}^+/\mathrm{H}^-)-E_{\mathrm{form}}(\mathrm{H}_T), \tag{3}$$

where $E_{\mathrm{form}}(\mathrm{H}^+/\mathrm{H}^-)$ is the formation energy of H^+ or H^-, and $E_{\mathrm{form}}(\mathrm{H}_T)$ is the formation energy of H in a deep trap state. The donor and acceptor levels of H in *c*-Si, located at ≈0.2 eV and ≈0.56 eV below the conduction band, respectively,[22] allow a determination of the relative formation energies of H^0, H^+, and H^-, and their dependence on E_F. As explained in Ref. 32 the relative formation energies can be placed on an absolute energy scale by referencing them to the energy of a free H atom. For the migration barrier for interstitial H diffusion we use the experimentally determined activation energy of $E_m=0.5$ eV for H diffusion in *c*-Si. Thus, the only unknown in Eq. (3) is $E_{\mathrm{form}}(\mathrm{H}_T)$.

The variation of $E_{\mathrm{form}}(\mathrm{H}_T)$ with the Fermi energy is shown in Fig. 22 for poly-Si and μc-Si. The zero of energy corresponds to a free H atom. The values are in the range of −2.2 to −2.6 eV where, according to first-principles calculations trapping states for H may occur.[32] For Fermi energies close to the conduction band values for $E_{\mathrm{form}}(\mathrm{H}_T)$ are lower by about 0.3 eV compared to E_F close to the valence band.

A careful look at the calculated energies for H configurations in *c*-Si reveals that all $E_{\mathrm{form}}(\mathrm{H}_T)$ values are located between the energy for H at an isolated Si dangling bond (−2.17 eV) and H accommodated at a Si dangling-bond in a vacancy (−3.15 eV).[32] However, an assignment of the formation energies of deep H trapping states to relevant H complexes cannot be made since the first-principle energies for H complexes such as H_2, H_2^*, and H at isolated dangling bonds are lower, while the energy for H at a pre-existing Si dangling-bond is much larger[32] than $E_{\mathrm{form}}(\mathrm{H}_T)$. For a thorough comprehension of $E_{\mathrm{form}}(\mathrm{H}_T)$ it is important to estimate the position of the hydrogen chemical potential and its influence on the diffusion process.

C. Hydrogen chemical potential

In analogy to the Fermi energy one can define a chemical potential for hydrogen, μ_{H}. The H chemical potential is independent of concentration over a large H concentration range; μ_{H} is pinned for most H concentrations[33] which is consistent with a negative-*U* model of H and the idea that H forms Si–H bonds in pairs. Pinning of μ_{H} occurs due to a reversed order of the single and double occupied states for H in silicon. The single occupancy configuration is positioned above μ_{H} and the zero and double occupancy states are located below μ_{H}.[34]

In Eq. (3) the migration barrier E_m and $E_{\mathrm{form}}(\mathrm{H}^+/\mathrm{H}^-)$ are independent of the H chemical potential. The only term that depends on μ_{H} is the formation energy of a deep H trap, $E_{\mathrm{form}}(\mathrm{H}_T)$. Therefore, the properties of $E_{\mathrm{form}}(\mathrm{H}_T)$ should be governed by μ_{H}. In Fig. 23 $E_{\mathrm{form}}(\mathrm{H}_T)$ is plotted as a function of the peak H concentration near the surface. In undoped poly-Si (diamonds) $E_{\mathrm{form}}(\mathrm{H}_T)$ changes about 0.2 eV when the H concentration is increased from the mid-10^{18} cm^{-3}

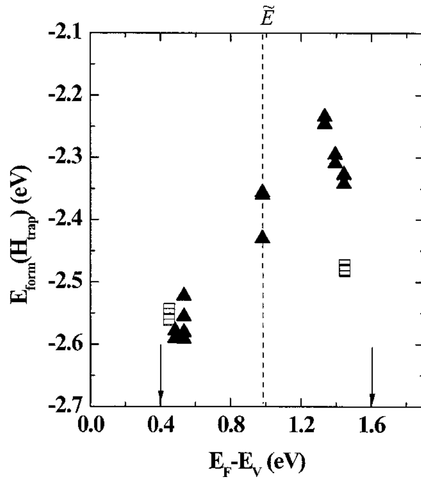

FIG. 22. Formation energy of H traps as a function of the Fermi energy. The data points were obtained by fitting the data of Fig. 20 to Eq. (3). The zero of energy corresponds to a free H atom. $\tilde{E}$ denotes the mean energy of the electronic states of H^+ and H^- in silicon. The arrows indicate the approximate positions of conduction and valence bands of poly-Si and μc-Si with respect to the band gap of *a*-Si:H.

level to about mid-10^{20} cm^{-3}. In P doped samples a smaller change of $E_{form}(H_T)$ of $\approx$0.1 eV is observed. On the other hand, in B doped poly-Si an increase of $E_{form}(H_T)$ with increasing H concentration is observed only for B concentrations smaller than 10^{17} cm^{-3}. At low H concentrations there is a clear difference between H diffusion in *p*-type and *n*-type poly-Si; according to Hall effect measurements nominally undoped poly-Si reveals *n*-type conductivity. In *p*-type poly-Si the formation energy for H trapping states $[E_{form}(H_T) \approx -2.5$ eV] is smaller than in *n*-type specimens $[E_{form}(H_T) \approx -2.4$ to -2.3 eV].

Assuming that H in the solid is in approximate equilibrium with the monatomic H in the plasma gas, then the quasichemical potential of the monatomic H gas, μ_{plasma}, determines the position of μ_H. The rate of change of μ_{plasma} with temperature amounts to $\mu_{plasma}/T = -0.0016$ eV/K.[8] Therefore, $E_{form}(H_T)$ should reveal a similar temperature dependence.

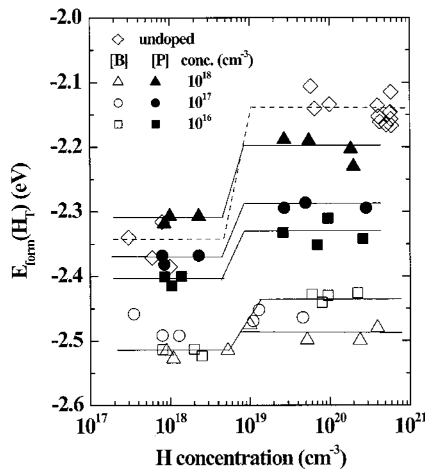

FIG. 23. $E_{form}(H_T)$ at 350 °C vs the peak H concentration near the sample surface.

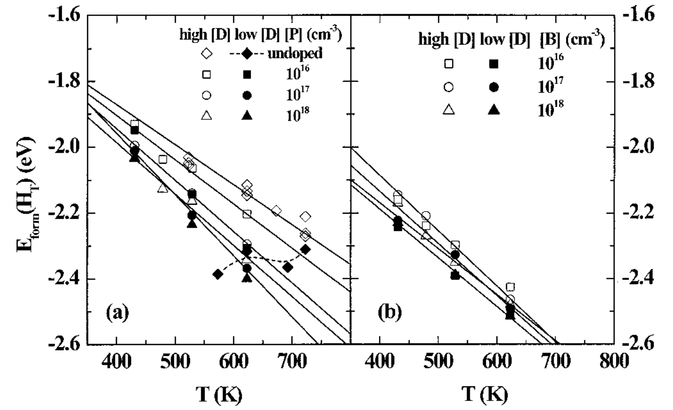

FIG. 24. $E_{form}(H_T)$ vs hydrogenation temperature, *T*, for (a) undoped and P doped poly-Si and (b) B doped poly-Si. The solid and open symbols represent low and high D concentration diffusion, respectively.

In Fig. 24 $E_{form}(H_T)$ is shown as a function of the hydrogenation temperature for the doping and passivation conditions described in the previous sections. Except for low D concentration diffusion into undoped poly-Si, which is represented by solid diamonds, $E_{form}(H_T)$ increases roughly at a rate of -0.0015 ± 0.0005 eV per K. This value agrees quit well with the rate of change of μ_{plasma} with temperature. The formation energy of deep H trapping states can be written as

$$E_{form}(H_T) = E_f^0(H_T) - kT \ln\left(\frac{N_H}{C_H}\right), \quad (4)$$

where $E_f^0(H_T)$ is the actual formation energy of deep H trapping sites, N_H is the density of H transport sites, and C_H is the concentration of H atoms residing in the transport states during the diffusion experiment. Using $E_f^0(H_T) = -1.65$ eV and $N_H \approx 10^{23}$ cm^{-3} the temperature dependence of $E_{form}(H_T)$ was calculated. The value of $E_f^0(H_T)$ corresponds to the first-principles energy for H_2^*.[32] In Fig. 25, fits and data of one B, one P, and the undoped poly-Si sample are shown. For clarity the other data sets shown in Fig. 24 were omitted in the plot. Fit and data are in excellent agreement. The only fitting parameter is C_H. In Fig. 26, C_H is plotted as a function of the Fermi energy. In *p*-type poly-Si ($E_F - E_V$ < 0.5 eV) C_H is in the range of 10^{16}–10^{17} cm^{-3} while in undoped and *n*-type samples C_H is about 1–2 orders of magnitude higher. A similar concentration of 10^{17} cm^{-3} H atoms in the transport states was observed in *in situ* conductivity measurements during plasma passivation of *p*-type poly-Si.[27] In addition, it is interesting to note an asymmetry in C_H comparing *n*-type and *p*-type poly-Si. This is reminiscent of the asymmetry of the formation energy of H^+ and H^- in *c*-Si.[23]

Assuming a simple two-level density-of-states, presented in Fig. 27, the position of the H chemical potential can be estimated. In Fig. 27 the migration saddle point is represented by the energy E_m which is considered to be roughly constant throughout disordered silicon. Below E_m is a distribution of shallow trapping sites near E_{BC/T_d}. In a micro-

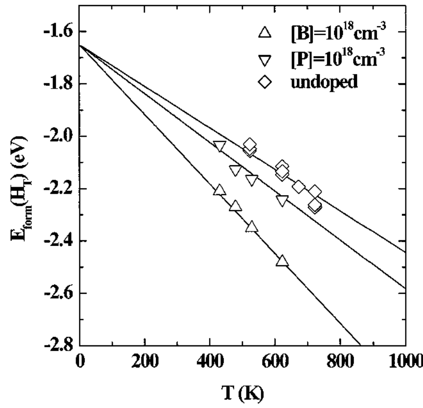

FIG. 25. Temperature dependence of $E_{\mathrm{form}}(\mathrm{H}_T)$. For clarity only three representative data sets of Fig. 24 and the corresponding fits are shown.

scopic picture these transport states correspond to Si-Si bond center and tetrahedral interstitial T_d sites in p-type and n-type material, respectively. As mentioned in Sec. IV B the height of the migration barrier depends on the charge state of H. However, like in the previous section we will use the experimental value of $E_m = 0.5$ eV.[26] Thus, the transport states E_{BC/T_d} are located around -1.05 eV. In equilibrium the H chemical potential separates the filled from the empty states. Hence, the H chemical potential resides between E_{BC/T_d} and $E_f^0(\mathrm{H}_T)$. This leads to an energy range of $\mu_{\mathrm{H}} = -1.1$ to -1.5 eV. An other estimate of μ_{H} can be obtained from the quasichemical potential of the monatomic H gas.[35] At a typical passivation temperature of 500 K and an atomic H concentration of 5×10^{15} cm^{-3} (Ref. 36), μ_{Plasma} amounts to ≈ 0.8 eV. Assuming that μ_{Plasma} in the near-surface region of the samples is approximately identical to μ_{H} the H chemical potential resides at approximately -1.35 eV at a hydrogenation temperature of 500 K, which is in good agreement with the energy range of -1.1 to -1.5 eV estimated above.

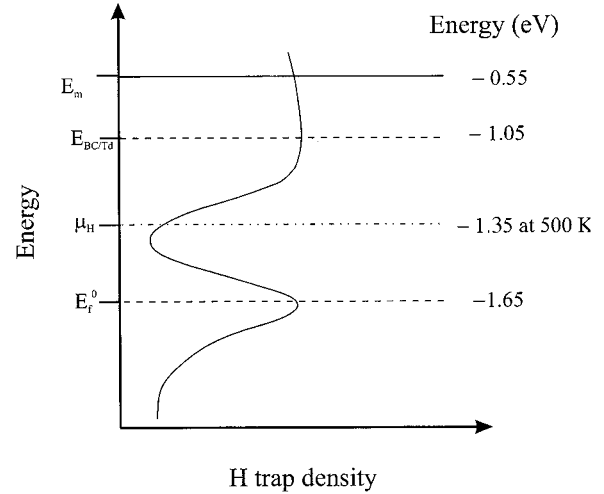

FIG. 27. Schematic H density-of-states distribution in disordered silicon. E_m, E_{BC/T_d}, and E_f^0 denote the energies of the migration saddle point, the Si–Si bond center position or the interstitial T_d site depending on the Fermi energy, and deep H trapping sites, respectively. The occupation of the various levels is determined by the H chemical potential, μ_{H}. The zero in energy corresponds to a free H atom.

V. SUMMARY

In summary, we have presented a detailed investigation on hydrogen diffusion in poly-Si and μc-Si. Hydrogen transport in doped poly-Si and μc-Si is enhanced compared to undoped material. The effective diffusion coefficient is thermally activated and varies between 0.01 and 1.69 eV in a response to a change of the H and dopant concentrations. The variation of E_A is accompanied by a change of the diffusion prefactor D_0 by more than 15 orders of magnitude. Using the theoretical diffusion prefactor the energy $\bar{E}_A$ necessary to yield the observed diffusion coefficient was calculated. The largest values for $\bar{E}_A$ were obtained for H diffusion in undoped poly-Si. Independent of the degree of disorder (a-Si:H, μc-Si, or poly-Si) $\bar{E}_A$ reveals a dependence on the Fermi energy similar to that of the formation energy of H^+ and H^- in c-Si. The data support a model for trap-limited H diffusion, in which $\bar{E}_A$ is the sum of the migration barrier for interstitial H and the H chemical potential, and the difference between the formation energies for a hydrogen interstitial (H^+ or H^-, depending on the Fermi energy), and for H at a deep trapping site $E_f^0(\mathrm{H}_T)$. An analysis of the experimental data yielded an energy of -1.65 eV for the H trapping site and the H chemical potential was estimated to reside at approximately -1.35 eV at a typical passivation temperature of 500 K.

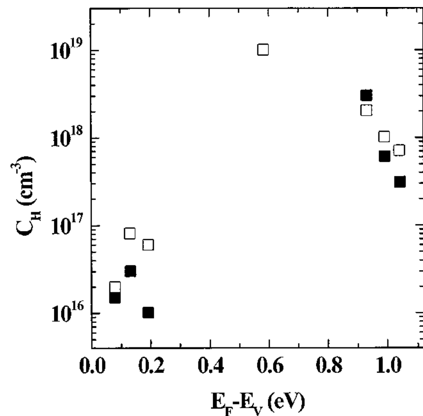

FIG. 26. Fitting parameter C_{H} as a function of the Fermi energy. The open and solid squares represent high and low D concentration diffusion, respectively.

ACKNOWLEDGMENTS

The authors wish to thank Dr. C. M. Jones who skillfully carried out the SIMS measurements at the Materials Analysis Group in Sunnyvale, CA. In addition, we are grateful to J. Krause and D. Patzek for technical support. This work was supported by the BMBF under Contract No. 0329773.

[1] N. H. Nickel, in *Hydrogen in Semiconductors II*, edited by N. H. Nickel (Academic, San Diego, 1999), Vol. 61, p. 83.
[2] N. M. Johnson, D. K. Biegelsen, and M. D. Moyer, Appl. Phys. Lett. **40**, 882 (1982).
[3] T. I. Kamins and P. J. Marcoux, IEEE Electron Device Lett. **EDL-1**, 159 (1980).
[4] M. J. Thompson, J. Non-Cryst. Solids **137&138**, 1209 (1991).
[5] C. H. Seager, in *Hydrogen in Semiconductors*, edited by J. I. Pankove and N. M. Johnson (Academic, San Diego, 1991), Vol. 34, p. 17.
[6] S. Ostapenko, L. Jastrzebski, and J. Lagowski, Appl. Phys. Lett. **68**, 2873 (1996).
[7] N. H. Nickel, N. M. Johnson, and W. B. Jackson, Appl. Phys. Lett. **62**, 3285 (1993).
[8] N. H. Nickel, W. B. Jackson, and J. Walker, Phys. Rev. B **53**, 7750 (1996).
[9] P. V. Santos and W. B. Jackson, Phys. Rev. B **46**, 4595 (1992).
[10] W. B. Jackson and C. C. Tsai, Phys. Rev. B **45**, 6564 (1992).
[11] N. H. Nickel, G. B. Anderson, and J. Walker, Solid State Commun. **99**, 427 (1996).
[12] N. H. Nickel, G. B. Anderson, N. M. Johnson *et al.*, Phys. Rev. B **62**, 8012 (1999).
[13] C. Herring and N. M. Johnson, in *Hydrogen in Silicon Semiconductors and Semimetals*, edited by J. I. Pankove and N. M. Johnson (Academic, San Diego, 1991), Vol. 34, Chap. 10.
[14] I. Beckers, N. H. Nickel, W. Pilz *et al.*, J. Non-Cryst. Solids **227–230**, 847 (1998).
[15] W. B. Jackson, N. M. Johnson, C. C. Tsai *et al.*, Appl. Phys. Lett. **61**, 1670 (1992).
[16] R. A. Street and C. C. Tsai, Philos. Mag. B **57**, 663 (1988).
[17] W. Beyer, in *Hydrogen in Semiconductors II*, edited by N. H. Nickel (Academic, San Diego, 1999), Vol. 61, p. 165.
[18] R. A. Street, C. C. Tsai, J. Kakalios *et al.*, Philos. Mag. B **56**, 305 (1987).
[19] W. Beyer, J. Herion, and H. Wagner, J. Non-Cryst. Solids **217–219**, 217 (1989).
[20] W. Meyer and H. Neldel, Z. Tech. Phys. (Leipzig) **18**, 588 (1937).
[21] W. Beyer, Phys. Status Solidi A **159**, 53 (1997).
[22] N. M. Johnson, C. Herring, and C. G. Van de Walle, Phys. Rev. Lett. **73**, 130 (1994).
[23] C. G. Van de Walle, P. J. Denteneer, Y. Bar-Yam *et al.*, Phys. Rev. B **39**, 10 791 (1989).
[24] N. M. Johnson, C. Doland, F. A. Ponce *et al.*, Physica B **170**, 3 (1991).
[25] J. I. Pankove and N. M. Johnson, in *Semiconductors and Semimetals*, edited by R. K. Willardson and A. C. Beer (Academic, San Diego, 1991), Vol. 34.
[26] A. Van Wieringen and N. Warmholtz, Physics **22**, 849 (1956).
[27] N. H. Nickel, N. M. Johnson, and J. Walker, Phys. Rev. Lett. **75**, 3720 (1995).
[28] N. M. Johnson, F. A. Ponce, R. A. Street *et al.*, Phys. Rev. B **35**, 4166 (1987).
[29] A. W. R. Leitch, V. Alex, and J. Weber, Phys. Rev. Lett. **81**, 421 (1998).
[30] C. G. Van de Walle and R. A. Street, Phys. Rev. B **49**, 14 766 (1994).
[31] N. H. Nickel and K. Brendel (unpublished).
[32] C. G. Van de Walle, Phys. Rev. B **49**, 4579 (1994).
[33] N. H. Nickel and W. B. Jackson, Phys. Rev. B **51**, 4872 (1995).
[34] S. Zafar and E. A. Schiff, Phys. Rev. B **40**, 5235 (1989).
[35] C. Kittel, *Thermal Physics* (Wiley, New York, 1969).
[36] N. M. Johnson, J. Walker, and K. S. Stevens, J. Appl. Phys. **69**, 2631 (1991).